Electro-optic effect in $BaTiO_3$ for spectral tuning of narrowband resonances

Da Shu, Evgeny Popov,* and Anne-Laure Fehrembach

Institut Fresnel, CNRS, Aix-Marseille University, Ecole Centrale Marseille, Campus de Saint Jerome, Marseille 13397, France
**Corresponding author: e.popov@fresnel.fr*

Received November 8, 2012; accepted January 9, 2013;
posted January 14, 2013 (Doc. ID 179551); published February 14, 2013

We study the electro-optic (E-O) properties of a $BaTiO_3$ thin layer placed in a stack of dielectric layers, including a subwavelength diffraction grating with a two-dimensional periodicity, aiming to tune spectrally the position of the resonant reflection peak that is used for narrowband optical filtering. $BaTiO_3$ is chosen due to its strong E-O properties. When an external electric field is applied to the E-O layer, it leads to a spectral shift of the resonant peak. We study numerically different configurations with either weak or strong spectral tunability, presenting some arguments to explain these different behaviors. Taking into account only the linear part of the E-O effect (Pockels effect), the tuning of the peak that has 0.1 nm spectral width is approximately 33 nm for a 1.5×10^7 V/m applied field. The shift is multiplied by three (97 nm) when also taking into account the quadratic E-O effect.

OCIS codes: 050.1950, 230.2090, 310.2790.

1. INTRODUCTION

Resonances in grating structures can be used for narrowband filtering, especially when using subwavelength gratings to excite guided-mode resonances in dielectric layers [1]. For a particular angle, polarization, and wavelength of incidence, this excitation can generate a resonance peak in the reflection and transmission spectra of the structure. The coupling condition writes

$$\|\vec{k}_{\mathrm{inc}} + \vec{K}\| \simeq k_g, \tag{1}$$

where $\vec{k}_{\mathrm{inc}}$ is the in-plane incident wave vector, $\vec{K}$ is a vector of the reciprocal space of the grating, and k_g is the propagation constant of the mode. A condition on the incident polarization is also required: the polarization of the incident field must not be orthogonal to that of the eigenmode. Very narrowband spectral filtering can be achieved with quite simple structures, and reflection efficiency can reach up to 100% if nonabsorbing dielectric materials are used [2,3]. Thus in the past decades, guided-mode resonance gratings became important components for many applications, such as optical narrowband filtering and sensing [4,5]. For some filtering applications, for example in telecommunications, the spectral tunability of the filter is required. The center wavelength of the peak of guided-mode resonant gratings can be controlled by modifying the period of the grating, the angle of incidence, or the optical index or the thickness of the layers. Only a few studies are reported on guided-mode resonance filters including an active layer [electro-optic (E-O), magneto-optic, etc.] [6–8]. They focus on the tunability performances in some configurations without a detailed analysis aiming at improving the tunability and other important properties, such as angular tolerance and polarization independence.

In this paper, our aim is to study, by the use of numerical modeling, a guided-mode resonance filter tuned spectrally by applying an external electric field to a layer of $BaTiO_3$, which is known for its strong E-O properties. We use a code based on the Fourier modal method [9] (also known as rigorous coupled-wave analysis). To our knowledge, this is the first numerical study of a 2D (periodic in two directions) guided-mode resonance filter that includes an E-O layer taking into account the anisotropy of the material. We first introduce the E-O properties of $BaTiO_3$ and the design of the structure under consideration. As a second step, we compare the behavior of different filter configurations and different orientations of the E-O material. Our main concern is the tunability of the filter structure, but we are also keeping in mind other important properties, such as the angular and the polarization sensitivity. Meanwhile, for our conclusions to be relevant, practical considerations (absorption losses, fabrications possibilities, etc.) are also discussed in the paper.

2. PRESENTATION OF THE STRUCTURE

A. Electro-Optic Properties of $BaTiO_3$ and Choice of Its Orientation

$BaTiO_3$, used throughout the paper as the E-O material, has a uniaxial anisotropy with extraordinary index $n_e = 2.43$ and ordinary index $n_o = 2.36$ at 1550 nm [10]. The components of the permittivity tensor of E-O materials change when they are subjected to an external electric field. $BaTiO_3$ in tetragonal state (below its Curie temperature 120°C) is characterized by both linear and quadratic E-O effects [10]. The nonlinear part is generally concealed by the linear effect. Hence, the quadratic effect in the ferroelectric tetragonal state of $BaTiO_3$ is usually neglected in applications, and even so, good comparisons between the simulations and the experimental results are obtained [11,12]. Yet, in resonant gratings, the

slightest variation in the index has to be multiplied by the period to obtain the variation on the resonant wavelength [see the coupling Eq. (1)]. Moreover, the order of magnitude of the quadratic coefficients [10] spur us on analyzing the influence of the quadratic effect. Note that above 120°C, $BaTiO_3$ exists in a paraelectric cubic state (point group symmetry m3m). This state is centro-symmetric, the Pockels effect is not present, and the quadratic effect is more important than in the tetragonal state.

Using the Voigt notation, the modifications of the index ellipsoid due to the Pockels effect and the quadratic effect in the tetragonal state of $BaTiO_3$ can be written as [13]

$$\left(\frac{1}{\tilde{\varepsilon}}\right)_i = \left(\frac{1}{\varepsilon}\right)_i + \sum_{k=1}^{3} r_{ik}E_k + \sum_{p=1}^{6} s_{ip}E_p^{(2)}, \tag{2}$$

where ε is the original relative permittivity of the material, expressed in its proper crystal axes (x_1, x_2, x_3) and r_{ik} and s_{ip} are the linear and the quadratic E-O coefficients, respectively. E_k is the k component of the applied electric field with index k going from 1 to 3, and $E_p^{(2)} = E_p^2$ for $p = 1$, 2, or 3, $E_4^{(2)} = 2E_2E_3$, $E_5^{(2)} = 2E_1E_3$, and $E_6^{(2)} = 2E_1E_2$. In Eq. (2), i goes from 1 to 6 and replaces the matrix indices ij, according to the rule given in Table 1.

The nonzero linear E-O coefficients of $BaTiO_3$ are $r_{33} = 28$ pm/V, $r_{13} = r_{23} = 8$ pm/V, $r_{51} = r_{42} = 1300$ pm/V. The nonzero quadratic coefficients of $BaTiO_3$ in the tetragonal state are [13] $s_{12} = s_{21}$, $s_{22} = s_{11}$, $s_{32} = s_{31}$, $s_{23} = s_{13}$, s_{33}, $s_{44} = s_{55}$, and s_{66}. To our knowledge the values for two coefficients only are reported in the literature [10], $s_{12} = -3.5 \times 10^{-17}$ m$^2 \cdot$ V^2 and $s_{32} = -8 \times 10^{-17}$ m$^2 \cdot$ V. Concerning the other coefficients, their implication depends on the mutual orientation between the crystal axes and the external electric field, as discussed in the next sections.

In the following, we will consider two different orientations of the $BaTiO_3$ crystal. The first one takes advantage of the largest linear E-O coefficient r_{42}, which is almost 50 times larger than the second one r_{33}. Thus, the axis x_2 (or alternatively x_1) must be collinear with the axis z along which the electric field is applied. We note it as the orientation 1. As we shall see in the next section, both the linear and the nonlinear E-O effect have a great influence on the tuning performance of the device in this orientation, which is characterized by optical anisotropy in the plane of the grating (extraordinary axis is lying in the Oyz plane).

Table 1. Reduced Notation for the Permittivity Tensor

i	1	2	3	4	5	6
ij	1,1	2,2	3,3	2,3	1,3	1,2

In the second orientation, the extraordinary axis of the crystal is parallel to the external electric field, so that the system becomes isotropic within the grating plane. This can help to obtain polarizationally independent response. The two other linear E-O coefficients r_{13} and r_{33} are implied, as well as the quadratic E-O coefficient $s_{13} = s_{23}$, and s_{33}. We note this design as orientation 2, and it will be discussed in Section 4.

B. Analysis of the Impact of Absorption Losses and Design of the Stack

As the final aims concern the filtering properties in reflection, this calls for a low sideband around the resonant peak; thus the entire device should represent a stack that forms an antireflection structure. Other important requirements that depend mainly on the grating parameters are the spectral bandwidth and the angular tolerances.

The principal layers of the structure are the E-O layer, the 2D grating, and the two ITO (indium-tin oxide) electrodes, necessary for applying the external voltage. Figure 1 shows three different filter designs. These configurations consist of several consecutive media, with two ITO layers, an HfO_2 air grating (reflective index of HfO_2 equal to $n = 1.9$), a buffer unetched HfO_2 layer between the grating and the E-O layer, a SiO_2 buffer layer between the E-O layer and the lower electrode (configurations 2 and 3), and a glass substrate. The main difference between the three configurations under study lies in introducing buffer layers between the electrodes and the guiding E-O layer. In order to obtain the greatest E-O effect with the lowest applied voltage, the first idea would be to put the electrodes close to the $BaTiO_3$ layer, as shown on Fig. 1(a). Yet, in practice, all the materials we use are lossless around 1550 nm, except for ITO [14,15]. In nonresonant devices, the losses in the ITO layers can be neglected, because the electrodes are optically quite thin. However, when resonant effects are used, even small values of extinction coefficients can lead to large absorption, in particular if the absorbing layers are put in the region of the device where the electromagnetic field of the guided mode is strong (configuration 1). In order to decrease the absorption, it is possible to remove the electrodes away from the guiding layer. This can be done by introducing a buffer layer between the

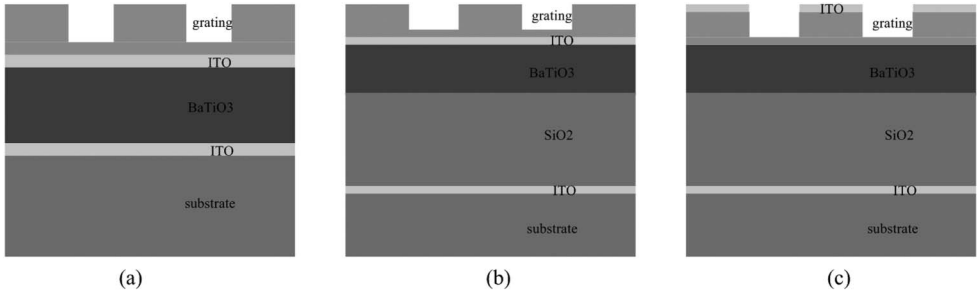

Fig. 1. Three different choices of the configuration: (a) configuration 1 with two ITO electrodes deposited directly on the E-O layer, (b) configuration 2 with a buffer layer of SiO_2 below, and (c) configuration 3 with SiO_2 buffer layer below and the grating structure acting as a buffer layer above.

Table 2. Influence of the ITO Absorption

Configuration	Index	Peak Position (nm)	Line Width (nm)	Efficiency (%)
1	$1.62 + 0.00i$	1570.2	0.06	100
	$1.62 + 0.01i$	1570.2	—	0.7
2	$1.62 + 0.00i$	1567.5	0.06	100
	$1.62 + 0.01i$	1567.6	0.1	1.7
3	$1.62 + 0.00i$	1569.9	0.09	100
	$1.62 + 0.01i$	1569.9	0.09	99.1
	$1.62 + 0.02i$	1569.9	0.092	97.3

electro-optical layer and the lower electrode (configuration 2). The upper electrode can be deposited over the grating structure before it is etched. This configuration is sketched in Fig. 1(c) and is addressed as configuration 3.

The grating structure has the same parameters for the three configurations, designed to enlarge the angular tolerances of the resonance, as explained further on. The $BaTiO_3$ is oriented with its extraordinary axis along y (first orientation).

The first study concerns the role of the losses of the electrodes on the resonant response of the device in configuration 1. When the grating parameters are suitably chosen to phase match the incident wave with one of the waveguide modes of the structure as discussed in Section 1, a peak in the reflectivity can be expected. And indeed, Fig. 2 shows that when the absorption of ITO is neglected, a narrow resonant peak occurs in the reflection spectrum and the maximum reaches 100% as expected from the symmetry considerations. However, the maximum is replaced by a minimum when the losses are taken into account, because the electrodes are attached to the high-index guiding layer of $BaTiO_3$. We take a TE mode as an example, but similar behavior is observed for TM modes or modes having higher modal number. Table 2 presents the spectral positions and the peak values of the resonant maximum due to the TE mode propagating in the x direction, for several different values of the relative permittivity of the ITO layers, and for the three different configurations. As can be observed, similar to configuration 1, the resonant peak in configuration 2 also disappeared when ITO absorption is taken into account. However, in configuration 3 with real losses [14,15], it is possible to obtain a maximum value of the reflectivity reaching 99.1%. Even when the imaginary part of the optical index is increased twice up to 0.02, the maximum value still can reach 97.3%. In what follows, we chose this configuration as the best filter structure. Another configuration for the electrodes has been proposed and experimentally studied

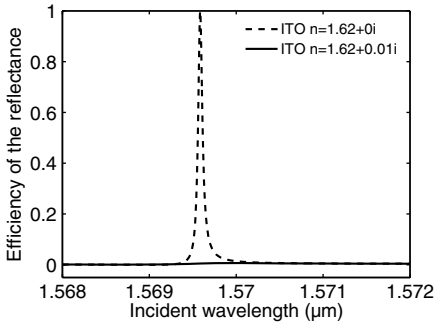

Fig. 2. Resonant peak of the configuration 1 in two different cases: dashed curve, ITO without absorption; straight line, ITO with absorption.

[16], however, presenting larger spectral linewidths and working at shorter wavelengths.

This configuration is detailed in Fig. 3(a). The thickness of each layer in the stack is chosen in order to form an antireflection coating outside the resonance. From top to bottom, we have 40 nm (ITO-air grating), 343 nm (HfO_2-air grating), 100 nm (HfO_2), 300 nm ($BaTiO_3$), 1000 nm (SiO_2), and 40 nm (ITO). The direction of the incident wave is defined using the polar angle θ and the azimuthal angle φ [Fig. 3(a)]. We choose the period in order to set the resonant peak of the fundamental TE mode located around 1550 nm. Figure 3(b) shows the top view of the grating pattern (one cell). The so called 2D doubly periodic pattern cell [17,18] has the same period $D = 762$ nm in the x and y directions in order to ensure simultaneous mode excitation in two orthogonal directions, aiming to a polarization independence of the system response. It contains four holes within each periodic cell with different diameters: diameter $D_1 = 293$ nm for both holes A and A', diameter $D_2 = 200$ nm for hole B, and $D_3 = 310$ nm for hole C. The previous papers [5,19] have proved that this designed pattern can increase the angular tolerances of the guided-mode resonance filter. This is due to the increased direct mode coupling between the modes excited in opposite directions. The increased direct coupling is provided through the second Fourier component of the grating profile, enhanced by the pairs of almost (but not completely) identical holes along each x- or y-direction.

The main difficulty in fabricating the devices we proposed is the problem of crystal growth on an amorphous material. Usually, $BaTiO_3$ crystal can grow on a substrate of MgO crystalline substrate, but this is not suitable for our purposes, partially because MgO has high optical index but mainly due to the necessity of introducing transparent electrodes (ITO, for example) between the substrate and the E-O layer, which completely neutralizes the structure similarity that enables crystalline growth. Whereas epitaxial growth may partially (but not fully) solve the manufacturing problem, a recent study proposes another method to overcome this difficulty. Bulk crystalline E-O material can be cut into a thin layer by wafer bonding and an ion slicing process (producing a 680 nm thin crystalline layer, in particular). This results in a material that can have electrodes, amorphous buffers, and other layers deposited on its surface [20]. This method has been applied to $LiNbO_3$; thus future works are required to study the possibility to apply this method to $BaTiO_3$.

3. TUNABILITY OF CONFIGURATION 3 FOR THE FIRST ORIENTATION OF $BaTiO_3$

In this section, we present the tunability performances for configuration 3, taking into account either only the linear

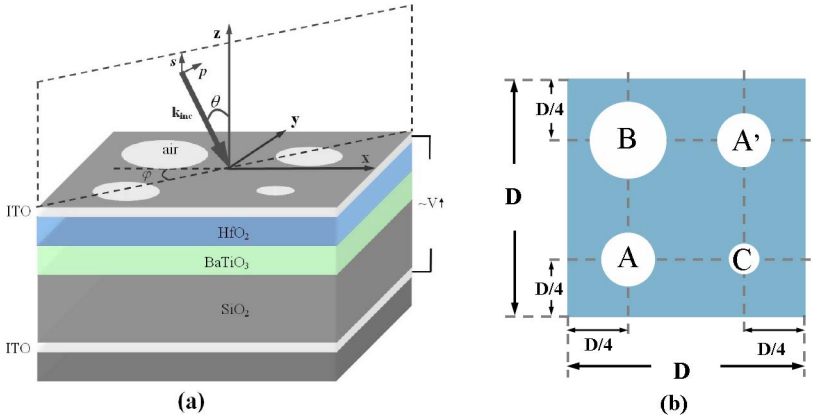

Fig. 3. (Color online) Description of the structure: (a) Stack of layers with indexes: HfO_2-air grating $n_1 = 1.9$, $n_0 = 1.0$; ITO $n_2 = 1.62$ at 1550 nm; $BaTiO_3$ $n_o = 2.43$, $n_e = 2.36$ at 1550 nm; and SiO_2 with $n_3 = 1.473$. (b) Top view of the component (one cell).

effect (case L) or both the combined linear and quadratic effects (case $L + Q$). We focus on the spectral shift of the resonance peak position as a function of the external electric field.

For the first orientation, the extraordinary axis of $BaTiO_3$ when no voltage is applied is oriented along the y direction, e.g., along one of the directions of periodicity of the grating. The permittivity tensor of the crystal with applied external electric field takes the following form in the (x, y, z) basis:

$$\tilde{\varepsilon} = \begin{pmatrix} \varepsilon_{xx} & 0 & 0 \\ 0 & \varepsilon_{yy} & \varepsilon_{yz} \\ 0 & \varepsilon_{zy} & \varepsilon_{zz} \end{pmatrix}. \tag{3}$$

As we consider that the E-O material is lossless, the permittivity tensor is Hermitian.

The external field modifies the coefficient ε_{xx} through the quadratic effect only. The other coefficients are modified due to both linear and quadratic effects. However, if the linear effect is not taken into account, the nondiagonal elements are null. The change of the different components of the permittivity tensor with respect to the applied voltage, varied within a range from -2 to 2×10^7 V/m, is plotted in Fig. 4.

Figure 4(a) shows the effect of the linear E-O coefficients only, and we see that when an external electric field is applied, two off-diagonal tensor elements ε_{yz} and ε_{zy} appear, so that the crystal becomes biaxial, with one axis of its index ellipsoid along x. Along the diagonal, ε_{xx} remains unchanged and the change of ε_{yy}, ε_{zz} have an approximately quadratic dependence on the electric field intensity. These changes lead to a modification of the waveguide mode frequencies and thus to a shift of the resonant wavelength. The filter will be tuned by the external electric field.

Figure 4(b) presents the variations of the elements of $\tilde{\varepsilon}$ versus the applied field intensity, as it was done in Fig. 4(a), but now taking into account both the linear and the quadratic terms in Eq. (2). There are several important differences between the figures (a) and (b). First, in (b), ε_{xx} varies with the applied field, contrary to the linear case. Second, the variations of the other elements are more than twice larger than when considering only the linear effect, except for ε_{zz}, which hardly changes when compared with the linear case. Third, the variation of the off-diagonal term is no more linear. However, the signs of the variations are the same as in linear case, so that we can expect the same directions of the shifts of the resonance wavelengths in the two cases.

A. Tunability Due to the Linear E-O Effect

We assume that the filter is illuminated by normally incident waves with s or p linear polarization (the electric field, respectively perpendicular or parallel to the plane of incidence). We consider a spectral range where there exist TE and TM modes propagating along the x or y direction (four modes). Because of the anisotropy of the $BaTiO_3$ in the xy plane, the TE modes have different constants of propagation along x and along y. The same is valid for the TM modes. Figure 5 illustrates the calculated reflectivity spectra for the TE mode propagating along x for different external electric field intensities in the

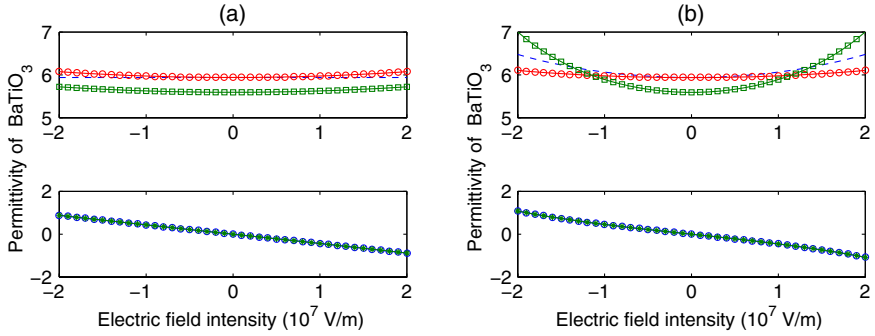

Fig. 4. (Color online) Variation of the permittivity tensor with the applied voltage taking into account either only the linear (a) or both the linear and the quadratic effects (b). ε_{xx}, ε_{yy}, ε_{zz} correspond, respectively to blue dash, green square, and red circle marks in the upper figures. ε_{yz}, ε_{zy} are presented as circles and stars in the lower figures.

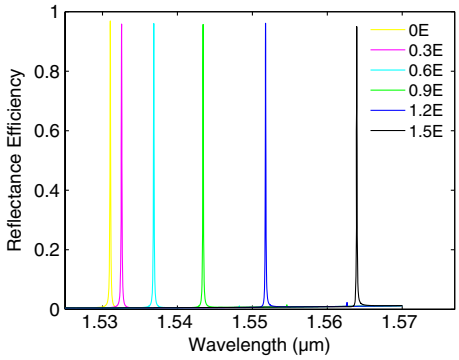

Fig. 5. (Color online) Simulated reflection spectra of TE mode along x direction versus the applied voltages due to the linear E-O effect.

case of linear E-O effect only (case L). As expected, the resonance peak shifts as the external field changes, which means that the concept of tunable resonant grating works.

A summary of the simulation results in this case is presented in Table 3. The first five columns indicate the incident polarization, the kind of mode excited in the structure (TE or TM), the center wavelength of the peak without applied voltage, and the full width at half-maximum (FWHM) of the resonance peak. The next two columns show the angular tolerances with respect to the polar incidence angle θ (see Fig. 3) when the incident wavevector lies in the xz plane and yz plane, respectively. In the last two columns, we give the shift of the peak center when the applied electric field changes from 0 to 1.5×10^7 V/m, and the maximum value of the reflection efficiency.

Concerning the angular tolerances, we observe in the table that they are quite different depending on whether the plane of incidence and the direction of excitation of the mode are mutually parallel or perpendicular. In the first case, the in-plane incident wavevector is collinear with the grating vector of the resonant order, so that the modulus of their vectorial sum in Eq. (1) varies more rapidly than if the two vectors are perpendicular to each other, as it happens when the plane of incidence is perpendicular to the direction of the mode. This explains the weaker angular tolerances in the collinear case as compared to the perpendicular one.

Concerning the shift of the peaks, let us first consider the TE mode excited along the x direction (in fact, as all the other cases under normal incidence, it consists of a standing wave constituted of two modes propagating in $+x$ and $-x$ direction). When the external field changes from 0 to 1.5×10^7 V/m, the peak shifts within 33 nm in the direction of the longer wavelength. The FWHM of the resonant peak remains almost constant close to 0.1 nm, which is an extremely narrow bandwidth. Meanwhile, the peak keeps low sideband levels (Fig. 5), which is very important for applications. The highest electric field intensity is lower than the dielectric breakdown for $BaTiO_3$, which roughly equals to 10^8 V/m [21], so even greater wavelength shift could be obtained by using higher static electric field. From this table we can also find that the TE mode along the x direction shows the strongest tunability, but the same mode along the y direction barely shifts under the same condition. On the other hand, the shift of the TM mode excited along x is 24.65 nm toward a shorter wavelength, while the shift of TM mode propagating along y is only 4.23 nm.

B. Explanation of the Shift Direction and Amplitude

From general principles, we can expect that the mode behavior is mainly influenced by the change of the elements of the permittivity tensor. In Fig. 6(a), we have plotted the shift of the resonant peaks for the modes listed in the Table 3 as a function of the applied field. The quasi-null shift of the peak of the TE mode along y (mode 2) can easily be understood since its electric field lies mainly along x, and ε_{xx} does not change when a static voltage is applied. To understand the evolution versus the applied voltage for the other modes, we have calculated the propagation constants of the modes of the equivalent planar structure, which consists of the same stack as the filter but with the last layer (grating) replaced by an homogeneous layer, with a permittivity in the (x, y) plane equal to the arithmetic mean of that of the grating, and the harmonic mean along z. Figure 6(b) presents the effective index of the modes of the equivalent planar structure as a function of the applied voltage, for the modes propagating in the x direction and y direction. Modes a, b, c, and d correspond to modes 1, 2, 3, and 4 of the grating structure (however, they are not exactly the same, as the modes of the grating structure 1–4 represent standing rather than propagating waves). We observe quite the same variations as in Fig. 6(a), which means that the peaks shift are mainly due to a modification of the modes propagation constant, rather than to a grating-induced effect. It has to be noted that the two less affected modes (2-b and 3-c) correspond to modes that remain purely TE and purely TM when the voltage increases, because ε_{xy}, ε_{yx}, ε_{xz} and ε_{zx} are null.

For the two other modes (1-a and 4-d) there is a mixing between the TE component and TM component because ε_{yz} and ε_{zy} are nonzero. As the electric intensity increases, the crystal becomes a biaxial anisotropic material, with one axis of its index ellipsoid along x, and the directions of the other axes varying in the Oyz plane. The components of the permittivity tensor of the crystal in its proper axis stand as an upper limit of the effective index of the modes that can propagate in this medium. Its components in the xy plane are the eigenvalues of the permittivity tensor (Eq. 3) and are given by

$$\varepsilon_{2,2/3,3} = \frac{\varepsilon_{yy} + \varepsilon_{zz}}{2} \pm \sqrt{\varepsilon_{yz}^2 + \left(\frac{\varepsilon_{yy} - \varepsilon_{zz}}{2}\right)^2}. \quad (4)$$

Table 3. Numerical Results for Configuration 3 in Case *L*

	Incident Polarization	Mode	Peak Center (nm)	FWHM (nm)	Angular Tolerance (xz) (°)	Angular Tolerance (yz) (°)	Peak Shift (nm)	Efficiency (%)
1	s	TE-x	1531.28	0.12	0.15	2.33	33.1	97.34
2	p	TE-y	1570.97	0.11	2.16	0.14	–0.08	97.31
3	s	TM-y	1456.76	0.40	4.08	0.35	4.23	61.02
4	p	TM-x	1461.40	0.41	0.34	3.88	–24.65	77.60

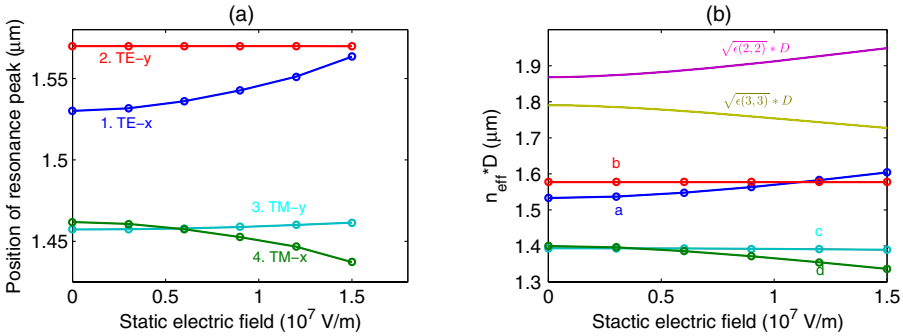

Fig. 6. (Color online) (a) Resonance peak wavelength position versus the external static voltage for TE and TM modes in configuration 3. (b) Violet and yellow curves $\varepsilon_{2,2}$ and $\varepsilon_{3,3}$ from Eq. (4), multiplied by the grating period D; the other curves show the mode effective index multiplied by D versus the external static voltage in the equivalent planar structure. Situations a, b, c, and d correspond to the resonances 1, 2, 3, and 4 in the Table 3.

The variation of $\sqrt{\varepsilon_{2,2}}$ and $\sqrt{\varepsilon_{3,3}}$ with the applied voltage is plotted in Fig. 6(b), too. In the absence of external field, $\varepsilon_{2,2} = \varepsilon_{yy} = n_e^2$. As far as the a-mode is due to the excitation of a quasi-TE mode along x, with electric field lying predominantly along y, it follows the variations of $\varepsilon_{2,2}$. The d-mode follows that of $\varepsilon_{3,3}$, because its electric field lies in the xz plane (quasi-TM mode excited along x) and is thus influenced by $\varepsilon_{3,3}$ and $\varepsilon_{x,x}$, the latter not changing. Equation (4) also explains the quadratic behavior of the shift versus the applied voltage (as well as the invariance with respect to its sign), since ε_{yz}, which is the only term linearly proportional to E_z, participates quadratically.

C. Tunability Due to Both Linear and Quadratic Effects

The influence of the quadratic E-O effect on the tunability of the device having the same configuration as in the previous subsection can be observed in Fig. 7, comparing it with the influence of the linear effect only. It presents the shift of the resonant peaks corresponding to the different modes listed in Table 3 as a function of the external electric filed intensity, separately for the linear effect and the combined linear and quadratic E-O terms. The coefficients implied are $s_{12} = -3.5 \times 10^{-17}$ m^2 V^{-2}, $s_{32} = -8 \times 10^{-17}$ m^2 V^{-2}, and s_{22}. We have considered that $s_{22} = 0$; yet we have checked that if s_{22} has the same order of magnitude as s_{12} and s_{32}, it does not lead to a significant modification of the propagation constant of the modes.

We see that the quadratic effect significantly increases the tuning range for some of the modes:

- for the mode 1, the shift is 97.30 nm in case $L + Q$, and 33.1 nm in case L,
- for the mode 2, the shift is 32.86 nm in case $L + Q$, and –0.08 nm in case L,
- for the mode 3, the shift is 13.51 nm in case $L + Q$, and 4.23 nm in case L,
- for the mode 4, the shift is –11.46 nm in case $L + Q$, and –24.65 nm in case L.

Contrary to the linear case, we observe a significant shift of the peak of the TE mode that propagates in the y direction, because of the variation of ε_{xx}. For the other modes, that involve the three coefficients ε_{yy}, ε_{zz}, and ε_{yz}, their behavior can be explained by the variation of the elements ε_{22} and ε_{33} of the permittivity tensor in the proper axes of the index ellipsoid, as it was done in the previous subsection. We have found that ε_{33} decreases less rapidly in the $L + Q$ case than in the L case, which explains the smaller shift of the quasi-TM-x mode. The most interesting case from a practical point of view is the stronger shift of the quasi-TE-x mode, which is related to the faster increase of ε_{22} in the $L + Q$ case. For this mode, the shift of the peak reaches 97.6 nm for 1.5×10^7 V/m applied external field (from 1531.3 to 1628.6 nm) without a visible change of its width which remains close to 0.1 nm. The spectral dependence of the reflectivity for different applied voltages, given in Fig. 8, confirms the magnitude of the spectral shift and the invariance of the form and width of the peak with respect to the applied voltage. It also confirms the almost quadratic dependence of the peak position, that directly follows from the results given in Fig. 7(a).

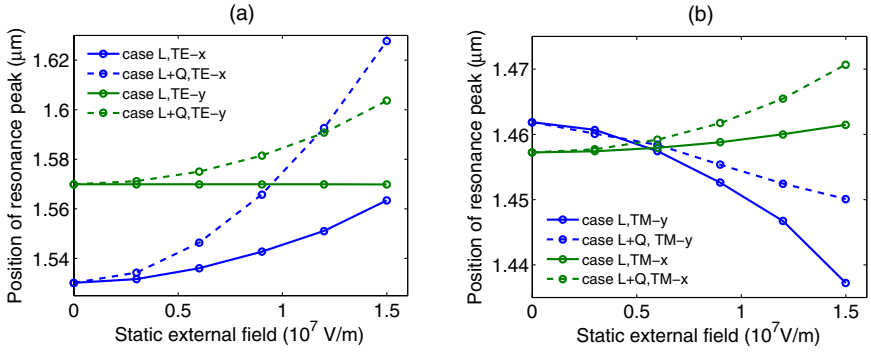

Fig. 7. (Color online) Resonant peak wavelength versus the external static voltage in configuration 3 for two different cases. Case L corresponds to the linear E-O effect only, in case $L + Q$ both linear and quadratic E-O effect are involved. (a) TE mode and (b) TM mode.

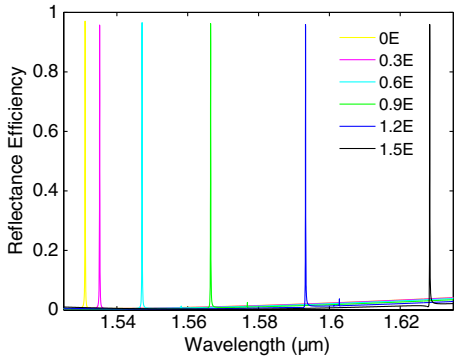

Fig. 8. (Color online) Simulated reflection spectra of TE mode along x direction versus the applied voltages due to the linear and quadratic E-O effect.

4. TUNABILITY OF CONFIGURATION 3 FOR THE SECOND ORIENTATION OF THE $BaTiO_3$

The first orientation of the $BaTiO_3$ crystal layer that has been chosen in the previous section uses the strongest linear E-O coefficient $r_{42} = 1300$ pm/V together with the second (in absolute value) quadratic coefficient $s_{12} = -3.5 \times 10^{-17}$ m^2 V^{-2}. Therefore, it was necessary to orient the extraordinary axis (x_3) of the crystal in the xy plane so that the static electric field acts along the ordinary axis. While this choice leads to a strong tuning effect (almost 100 nm), the price to be paid is the anisotropy in the xy plane, which makes it impossible to make a polarization-independent device. While the strong dependence of the response versus the incident polarization is not a handicap in applications where the narrowband reflection filters act as mirrors for tuning of the lasing wavelength of lasers, devices used in spectroscopy (e.g., space-born environmental monitoring) or in telecommunication (wavelength demultiplexing) require low polarization dependent losses.

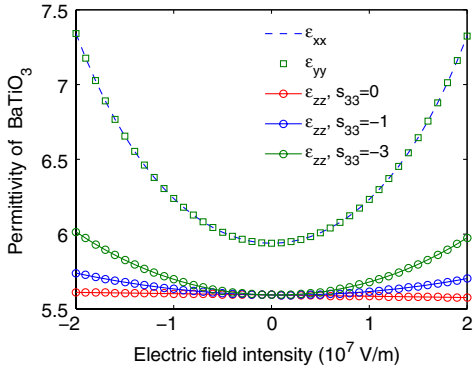

Fig. 9. (Color online) Permittivity tensor elements of $BaTiO_3$ in the case of second orientation with three different values of the quadratic coefficient s_{33}.

Such polarization independence can be achieved by using the orientation 2, as already defined, in which the extraordinary axis is oriented in the vertical (z) direction. By applying the external electric field in the same direction, the configuration will impose the use of the linear and nonlinear E-O coefficient having 3 as a second index. These are $r_{13} = r_{23} = 8$ pm/V, $r_{33} = 28$ pm/V, $s_{13} = s_{23} = -8 \times 10^{-17}$ m^2 V^{-2}, and finally s_{33}, which is unknown. We follow the hypothesis made in [10] [Eq. (12)] that $s_{13} = s_{31}$. Concerning s_{33}, in what follows, we have tried three different values, with the same order of magnitude as the other coefficients.

The values of the linear coefficients are much lower than in orientation 1; however, the nonlinear coefficient s_{13} involved in orientation 2 is more than twice greater than s_{12}, participating in orientation 1. The variation of the elements of the permittivity tensor with the external electric field in orientation 2 can be observed in Fig. 9. The strongest variation concerns the diagonal elements $\varepsilon_{xx} = \varepsilon_{yy}$, variations that are comparable with those of ε_{yy} in Fig. 4(b), so that we can expect similar tuning range of the TE-mode, for which the electric field lies in the grating plane and is affected mostly by the changes in ε_{xx} and/or ε_{yy}. In addition, their equality will ensure the polarization independence of the device, because in this orientation, due to the isotropy in the xy plane, the modes excited in different directions have the same constants of propagation and are linearly polarized. In particular, if we excite a TE mode in direction of the x axis with an incident wave polarized along the y axis, an incident polarization along the x axis can excite the same TE mode in y direction under the same conditions, i.e., the resonance anomaly will appear at the same wavelength, at least in normal incidence.

A. Tunability

The spectral dependence of the resonance peak due to the TE mode is shown in Fig. 10 for two different values of the tuning electric field, and taking into account the losses in the ITO electrodes. Both s and p polarized incident waves have the same spectral response (as a direct consequence of the

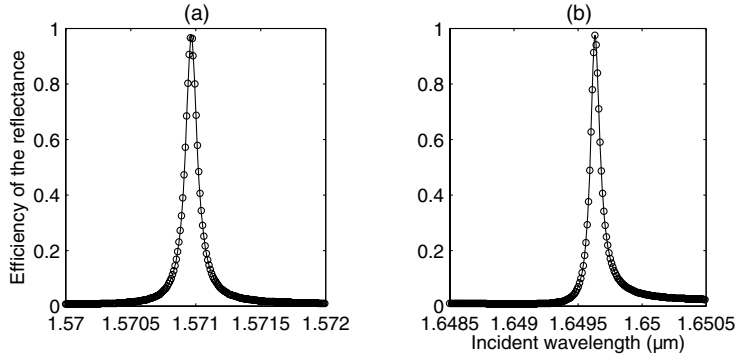

Fig. 10. Resonant peak for the second orientation with ITO layer absorption taken into account. The maximum of reflective efficiency reaches 97.3%. (a) Without external electric field and (b) with 1.5×10^7 V/m electric field.

Table 4. Numerically Computed Results of the Second Orientation in Three Cases

Case ($\times 10^{17}$)	Mode	Peak Position (nm) for 0 V · m^{-1}	FWHM (nm) for 0 V · m^{-1}	FWHM (nm) for 1.5×10^7 V · m^{-1}	Peak Shift (nm) −0.48	Efficiency (%)
L	TE	1570.97	0.11	0.11		97.41
L	TM	1441.03	0.40	0.39	−0.94	59.45
$L + Q\ s_{33} = 0$	TE	1570.97	0.11	0.10	78.66	97.55
$L + Q\ s_{33} = 0$	TM	1441.03	0.40	0.41	7.5	60.12
$L + Q\ s_{33} = -1$	TE	1570.97	0.11	0.10	78.78	97.54
$L + Q\ s_{33} = -1$	TM	1441.03	0.40	0.42	12	60.02

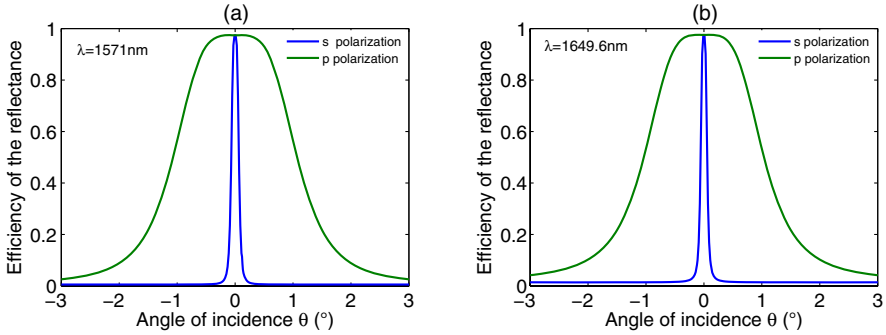

Fig. 11. (Color online) Angular tolerance of the second orientation under the condition of no external electric field and with 1.5×10^7 V/m intensity. The incident plane wave varies in the xz plane.

isotropy in the xy-plane), with spectral width of the maxima practically independent of the tuning electric field.

Table 4 summarizes the E-O effects' influence on the resonant peak characteristics in orientation 2. The first two lines take into account the linear part only. As can be observed, the tuning is much less pronounced than in orientation 1, because the linear coefficients that participate now are almost 50 times smaller than in orientation 1. The isotropy in the xy plane skips the necessity to separately treat the mode exited in x or y direction. The next lines of the table present the results of both the linear and quadratic E-O effect. As s_{33} is unknown to us experimentally, we have tried two different values, 0 and -1×10^{-17} m^2 V^{-2}, with the corresponding variations of ε_{zz} plotted in Fig. 9. As these variations are relatively small, the influence of s_{33} within the chosen range of uncertainty is negligible for the TE mode (that has no electric field along z), as observed in Table 4. On the contrary, the tuning of the TM mode is strongly dependent on the choice of s_{33}. However, from a practical point of view the TE mode is more interesting, because of its larger tuning range. It is about 20% smaller than the maximum tuning range in orientation 1, but there is a compensation obtained in the form of polarization independence. The shift toward greater wavelength can be explained by the fact that in this configuration, the index ellipsoid does not rotate when an electric field is applied; its diagonal elements increase (see Fig. 9), which leads to an increase of the effective index of the guided modes, thus to an increase of the resonance wavelength.

B. Angular Dependence

Finally, Fig. 11 represents the angular dependence of the same resonance due to the TE mode excitation, when the incident angle is varied within the xz plane. For one of the incident polarizations, the mode excitation is made in one direction, while for the other, the grating excites the mode in a direction perpendicular to the first mode direction; thus the angular conditions of excitation as provided by Eq. (1) are quite different.

For a mode excited in a direction perpendicular to the plane of variation of the incident angle, the modulus of the sum of the horizontal component of the incident wavevector with the grating vector varies less rapidly than if the two vectors are collinear, which determines the different angular responses with respect to the incident polarization. Given the variation of the incident angle in the other plan (yz), the angular dependencies are interchanged. Thus, strictly speaking, when going out of normal incidence (or working with divergent or convergent beams), the device is not completely polarization independent. However, this is also valid for the filters based on resonant gratings with no possible tuning. Moreover, as seen in Fig. 11(b), the angular tolerances are only slightly worsen due to the tuning. Without external field the angular widths at half-maximum are $\Delta\theta_s = 2.16°$, $\Delta\theta_p = 0.13°$, values that decrease slightly under 1.5×10^7 V/m external field: $\Delta\theta_s = 2.09°$, $\Delta\theta_p = 0.12°$.

5. CONCLUSION

We have studied numerically a guided mode resonance filter containing an E-O $BaTiO_3$ layer, and compared the tunability of resonances based on the excitation of different kinds of guided modes with different polarizations, for two orientations of the crystal. Whatever the configuration, we have observed that the shift of the resonance peaks corresponds to the variation of the effective index of the guided mode of the equivalent planar structure (without grating).

In the first orientation the crystal is anisotropic in the plane of the grating and the index ellipsoid rotates when an electric field is applied, and we have obtained strong or weak variations, toward greater or smaller wavelengths. We have shown that a strong tunability occurs when the modes become hybrid

(neither pure TE nor pure TM) with the increase of the applied voltage. In fact, the propagation constants of the hybrid modes vary, with respect to the applied voltage, in a similar manner as the indexes of the biaxial anisotropic material in its proper axes. These indexes can either decrease or increase, leading to a shift of the resonance peak toward greater or smaller wavelengths. The same conclusions stand when taking into account the linear (Pockels) effect only, or both linear and quadratic effects. We obtain almost 98 nm tunability (33 nm if the quadratic effect is neglected) for a peak with Q factor of 15,000 with maximum applied field intensity 1.5×10^7 V/m that is below the $BaTiO_3$ breakdown. The anisotropy of the structure leads, as expected, to a dependence of the peak with respect to the polarization of the incident wave. All these points show the importance of taking into account the anisotropy of $BaTiO_3$ in the simulations.

For the second orientation (with the crystal isotropic in the plane of the grating whatever the applied voltage), the peaks shift toward greater wavelengths following the variation of the permittivity tensor elements. The maximum tunability obtained is almost 79 nm for a peak with Q factor of 15,000 with the same maximum applied field intensity of 1.5×10^7 V/m. This is smaller than the tunability obtained for the first orientation of the crystal, but the advantage is that the peak is polarization independent in this configuration.

We believe that this detailed study of $BaTiO_3$ based guided-mode resonance filter paves the way to further studies, including experimental studies, particularly as we have shown that the deterioration of the spectral selectivity and efficiency caused by the absorption losses of ITO can be reduced by choosing a suitable design.

REFERENCES

1. L. Mashev and E. Popov, "Zero order anomaly of dielectric coated gratings," Opt. Commun. **55**, 377–380 (1985).
2. E. Popov and E. Bozhkov, "Corrugated waveguides as resonance optical filters advantages and limitations," J. Opt. Soc. Am. A **18**, 1758–1764 (2001).
3. A.-L. Fehrembach, D. Maystre, and A. Sentenac, "Phenomenological theory of filtering by resonant dielectric gratings," J. Opt. Soc. Am. A **19**, 1136–1145 (2002).
4. R. Magnusson, D. Shin, and Z. S. Liu, "Guided-mode resonance Brewster filter," Opt. Lett. **23**, 612–614 (1998).
5. A. Mizutani, H. Kikuta, and K. Iwata, "Wave localization of doubly periodic guided-mode resonant grating filters," Opt. Rev. **10**, 13–18 (2003).
6. H. Ichikawa and H. Kikuta, "Dynamic guided-mode resonant grating filter with quadratic electro-optic effect," J. Opt. Soc. Am. A **22**, 1311–1318 (2005).
7. A. Sharon, D. Rosenblatt, A. A. Friesem, H. G. Weber, H. Engel, and R. Steingueber, "Light modulation with resonant grating waveguide structures," Opt. Lett. **21**, 1564–1566 (1996).
8. T. Katchalski, G. Levy-Yurista, A. A. Friesem, G. Martin, R. Hierle, and J. Zyss, "Light modulation with electro-optic polymer-based resonant grating waveguide structures," Opt. Express **13**, 4645–4650 (2005).
9. L. Li, "New formulation of the Fourier modal method for crossed surface-relief gratings," J. Opt. Soc. Am. A **14**, 2758–2767 (1997).
10. M. Melnichuk, "Method for measuring off-diagonal Kerr coefficients by using polarized light transmission," J. Opt. Soc. Am. A **22**, 377–384 (2005).
11. A. Petraru, J. Schubert, M. Schmid, and Ch. Buchal, "Ferroelectric BaTiO3 thin-film optical waveguide modulators," Appl. Phys. Lett. **81**, 1375–1377 (2002).
12. P. Tang, D. J. Towner, T. Hamano, and A. L. Meier, "Electro-optic modulation up to 40 GHz in a barium titanate thin film waveguide modulator," Opt. Express **12**, 5962–5967 (2004).
13. A. Yariv and P. Yeh, *Optical Waves in Crystals* (Wiley, 1984).
14. S. Laux, N. Kaiser, A. Zöller, R. Gützelmann, H. Lauth, and H. Bernitzki, "Room-temperature deposition of indium tin oxide thin films with plasma ion-assisted evaporation," Thin Solid Films **335**, 1–5 (1998); see also http://www.luxpop.com.
15. L.-J. Meng and F. Placido, "Annealing effect on ITO thin films prepared by microwave-enhanced dc reactive magnetron sputtering for telecommunication applications," Surf. Coat. Technol. **166**, 44–50 (2003).
16. S. A. Kemme, R. R. Boye, D. W. Peters, and R. O. Nellums, "Active resonant subwavelength grating for scannerless range imaging sensors," Proc. SPIE **6469**, 646906 (2007).
17. A.-L. Fehrembach, A. Talneau, O. Boyko, F. Lemarchand, and A. Sentenac, "Experimental demonstration of a narrowband, angular tolerant, polarization independent, doubly periodic resonant grating filter," Opt. Lett. **32**, 2269–2271 (2007).
18. A.-L. Fehrembach, F. Lemarchand, and A. Talneau, "High Q polarization independent guided-mode resonance filter with 'doubly periodic' etaced Ta_2O_5 bidimensional grating," J. Lightwave Technol. **28**, 2037–2044 (2010).
19. F. Lemarchand and A. Sentenac, "Increasing the angular tolerance of resonant grating filters with doubly periodic structures," Opt. Lett. **23**, 1149–1151 (1998).
20. P. Rabiei and P. Gunter, "Optical and electro-optical properties of submicrometer lithium niobate slab waveguides prepared by crystal ion slicing and wafer bonding," Appl. Phys. Lett. **85**, 4603 (2004).
21. K. Sreenivas, A. Mansingh, and M. Sayer, "Structural and electrical properties of rf-sputtered amorphous barium titanate thin films," J. Appl. Phys. **62**, 4475–4481 (1987).